Reaction path modelling illustrating the fluid history of a natural CO_2-H_2S reservoir

Carmen Zwahlen, Roy Wogelius, Cathy Hollis, Greg Holland

Abstract

Despite the increasing interest in geologic co-sequestration of CO_2 and H_2S, the long-term consequences of the chemical interactions involved in this process remain largely unknown on a reservoir scale. A Mississippian aged CO_2-H_2S reservoir in LaBarge Field, Wyoming, USA is an ideal study site to investigate mineral and fluid reactions related to gaseous H_2S and CO_2. We conducted two reaction path models based on mineralogical, fluid, gas, and stable isotope compositional data to discern the role of CO_2 influx upon the generation of H_2S through thermochemical sulphate reduction (TSR). We discriminate between two models- one in which TSR is triggered by temperature at a given burial depth and one where TSR is triggered by ingress of CO_2. The reaction path model based upon burial-controlled TSR and later CO_2 influx is consistent with mineralogical observations and stable isotope measurements from drill cores. The models show that CO_2 influx leads to calcite precipitation which is only limited by the calcium concentration in the fluid. This modelling approach is useful in constraining the timing of fluid flux in the reservoir and gives further insight into the mineralogical consequences of the gas, water, and rock interactions occurring in the reservoir. In terms of geologic co-sequestration this implies that the addition of CO_2 into a reducing carbonate system can result in calcite precipitation, instead of anhydrite as previously thought. Furthermore, it is only limited by the availability of Ca^{2+} and will therefore not diminish the amount of H_2S in the system.

Introduction

Natural oil and gas reservoirs can give insight into key processes acting over geological timescales (Allis et al., 2001; Bickle et al., 2013; Kampman et al., 2014; Kaszuba et al., 2011). Additionally, knowledge of the H_2S concentration in reservoirs is of interest for drilling safety and gas degradation. It is important to understand the fluid history in these reservoirs in order to predict which reactions can occur and to what extent. In particular, there is increasing interest in the feasibility of geologic co-sequestration of CO_2 and H_2S within carbonate systems (Kaszuba et al., 2011; Williams & Paulo, 2002). The long term consequences, however, are difficult to predict using lab and field experiments or geochemical reaction modelling alone.

The CO_2-H_2S reservoir in LaBarge Field, southwestern Wyoming, USA, has been classified and studied as a natural analogue for geological co-sequestration (Allis et al., 2001; Kaszuba et al., 2011) (Figure 1). The gas trapped in LaBarge Field consists on average of 66% CO_2, 21% CH_4, 7% N_2, 5% H_2S and 0.6% He (Huang et al., 2007). The H_2S is thought to be produced by thermochemical sulphate reduction (TSR) whereas the CO_2 is believed to be from a magmatic source (De Bruin, 1991, 2001; Huang et al., 2007; Stilwell, 1989; Zwahlen et al., 2019). However the timing of the fluids remains controversial. Hydrocarbons are thought to have migrated into the reservoir approximately 84 -76 Ma ago (Johnson, 2005) (Figure 2). Different techniques and data sets have been employed to study the influence of CO_2 and H_2S upon each other (Huang et al., 2007; Kaszuba et al., 2011; Obidi, 2014; Zwahlen et al., 2019): diffusion modelling of the CO_2-CH_4 distribution concluded that hydrocarbon and CO_2 were introduced at similar times, around 50 Ma ago (Huang et al., 2007) and reaction path modelling has been used to suggest that TSR was triggered by the influx of CO_2 (Kaszuba et al., 2011). In contrast, a more complex diffusion model, using the same CO_2-CH_4 distribution, suggests a larger time gap of >45 Ma between the CH_4 and CO_2 influx, with the CO_2 arriving <3 Ma ago (Obidi, 2014). Mineralogical observations and stable isotope measurements also suggest a two step process in which CO_2 arrived later (Zwahlen et al., 2019). In this paper, we build a geochemical model that is informed by petrographical and geochemical observations to further constrain the fluid history in

LaBarge Field. This will improve our understanding of the mineralogical consequences of the CO_2 influx, the initiation of TSR and hence the H_2S generation in the carbonate reservoir.

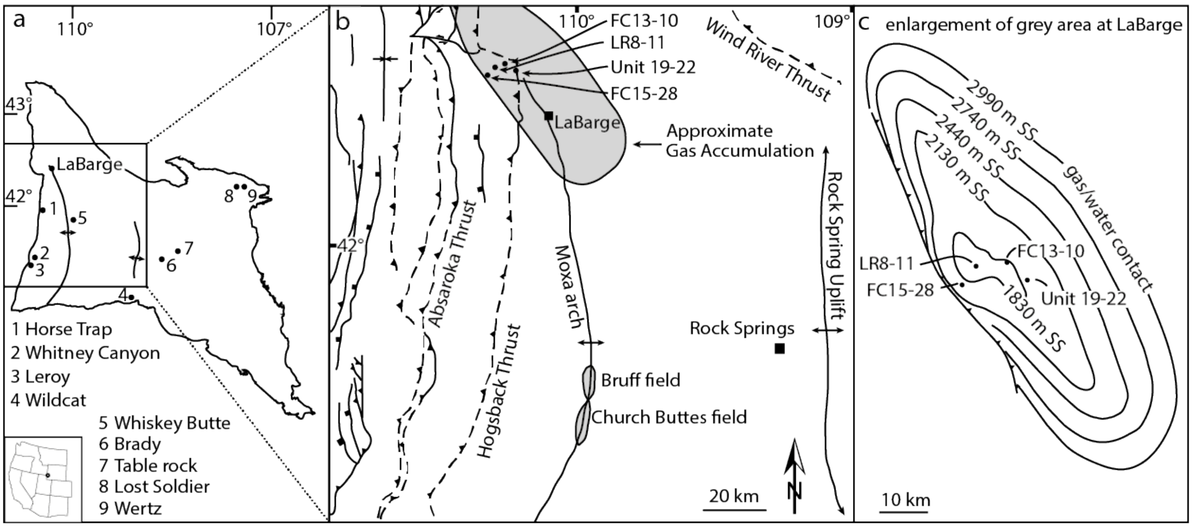

Figure 1 a) Map of greater green river basin with marked fluid sample localities b) Map of the CO_2- H_2S reservoirs along the Moxa arch and main tectonic features in the area modified after Becker and Lynds, (2012). c) The LaBarge Field with sampling wells modified after (Stilwell, 1989).

We conducted two different reaction path models: Model 1 involved a two step process where burial related TSR occurred and CO_2 ingress occured later (Figure 3). Model 2 assumed TSR was triggered by the CO_2 influx (Figure 3). The two different scenarios also occurred at different temperatures. The CO_2 is thought to have entered the reservoir at the maximal burial temperature, estimated to be 200 to 215 °C (Zwahlen et al., 2019), whereas burial related TSR is thought to have started around 175 °C based on fluid inclusion microthermometry data (Zwahlen et al., 2019). Using a simple titration model of the organosulphur compound methionine(aq) and CO_2(g) we simulated TSR and CO_2 input into the reservoir, respectively (Figure 3). This approach could be applied to other systems in order to improve the understanding of their fluid history and the long-term fate of the presence of a reactive gas such as H_2S.

Figure 2 Burial history of the Madison Formation at LaBarge modified after Roberts et al., (2005) and adapted to 500 m further uplift at LaBarge in the last 5 Ma. The Madison Formation is highlighted in grey. Fm., Formation; Sh., Shale; Gp., Group; Ss., Sandstone; L. Cret., Lower Cretaceous rocks.

Figure 3 Schematic of model 1 & 2 including reaction temperature and aimed mineral precipitates.

Mineralogy and paragenesis of LaBarge

The Mississippian Madison Formation in LaBarge Field consists of limestone, that was deposited in shallow water, interlayered with dolomite that formed during shallow burial, and former anhydrite nodules that were replaced by calcite (Figure 4). A similar succession has been observed in other parts of Wyoming, USA (Budai & Cummings, 1987; Budai, 1985; Budai et al., 1984; Buoniconti, 2008; Katz, 2008; Katz et al., 2007; Smith et al., 2004; Sonnenfeld, 1996). The following summary of the paragenetic sequence in LaBarge Field has been established by petrographic observations, stable isotope and fluid inclusion microthermometric analysis (Zwahlen et al., 2019). The carbon and oxygen isotopic signatures measured on whole rock limestone and dolostone are consistent with other measurements of the Mississippian Madison Formation in Wyoming (e.g. Budai and Cummings, 1987; Katz et al., 2006)(Figure 5). Calcite cements fill primary and secondary matrix macropores. Thereafter, quartz, fluorite and fracture filling calcite precipitated in sequence from hydrothermal fluids that cooled during fluid circulation and mineral precipitation. This is supported by decreasing primary fluid inclusion homogenisation temperatures within single quartz crystals from core to rim (145 - 110 °C), by primary fluid inclusion homogenisation temperatures in fluorite of 105-110 °C and carbon and oxygen isotopic values of the fracture filling calcite phase that show equilibration with the host rock (Figure 4c & 5). After the fracture filling calcite precipitation, hydrocarbons seeped into the system at 84-76 Ma ago (Roberts et al., 2005). The last precipitating carbonate mineral phase is the calcite that replaces anhydrite, which has primary fluid inclusion homogenisation temperatures between 175-200 °C (Figure 4d & e). This is interpreted to have occurred during thermochemical sulphate reduction, also leading to precipitation of pyrite, elemental sulphur and solid bitumen (Figure 4d & f). There is no primary anhydrite left except for micro inclusions in the calcite nodules (Figure 4e). The distinctive, depleted carbon and oxygen isotopic values of these samples are in consistent with an isotopically light carbon source, which could either be hydrocarbon or carbon dioxide, and with the elevated precipitation temperatures (Figure 5).

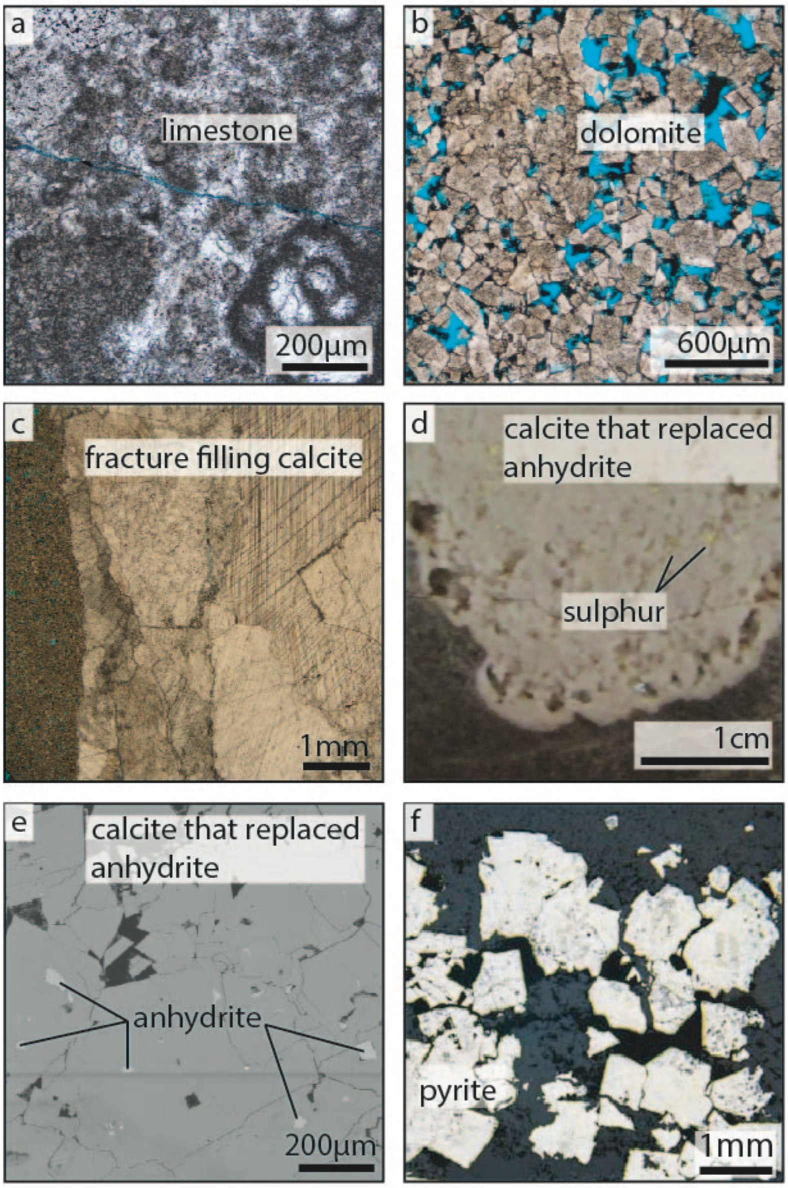

Figure 4 a) Mississippian limestone and b) dolomite host rock. c) Fracture filling calcite d) Former anhydrite nodule that was replaced by calcite with elemental sulphur precipitated between calcite crystals e) Remaining anhydrite microinclusions in calcite that replaced anhydrite f) pyrite

Figure 5 Carbon and oxygen isotopic data from carbonate samples. Black, grey and white symbols represent samples from drill core FC13-10, LR8-11 and FC15-28 respectively. Data is from (Zwahlen et al., 2019).

Model input data and constraints

The two different titration models are based on gas, mineralogical and fluid compositional data from four boreholes at the centre of the reservoir (Blondes et al., 2016; Huang et al., 2007; Zwahlen et al., 2019) (Figure 1). Therefore, the reservoir conditions are calculated for this part of the field. The reservoir temperature is calculated to be 133 °C based on an average maximum depth of the four drill cores, 4612 m, and a geothermal gradient of 28.8 °C/km (Roberts et al., 2005). According to bottom hole pressures the gas pressure is on average 450 bar for the four bore holes and identical to hydrostatic pressure (Becker & Lynds, 2012).

The model was further constrained by mineralogical data from three drill cores (LR8-11, FC15-28 and FC13-10, Figure 1B & C). The model is set up for 1 kg of water. Based on a density of 1 kg/dm^3 and a porosity of 9% (Huang 2007) this water would fill a rock volume of 10111 cm^3. The host rock is composed of dolomite (~60%) and limestone, however, in the model we use dolomite as a sole host-rock condition (10091 cm^3) to avoid over-constraining the system (Zwahlen et al., 2019). The estimated volume of calcite that replaced anhydrite in the drill cores is 0.2 vol% which equates to 20 cm^3 (Zwahlen et al., 2019). The pH in the carbonate reservoir is likely governed by calcite and dolomite. The original fluid at 133 °C with the pH set in equilibrium with either dolomite or calcite results in a pH of 5.5 to 5.7 and therefore we choose a starting pH of 5.6.

H_2S fugacity was used as a constraint for the oxygen fugacity of the model. The H_2S fugacity can be calculated based on the gas composition, the total gas pressures and the fugacity coefficient:

$$f_{H_2S(g)} = P * x_{H_2S(g)} * \varphi_{H_2S(g)} \quad (1)$$

where $f_{H2S(g)}$ is the gas fugacity, P the total pressure, $x_{H2S(g)}$ the mole fraction of H_2S and $\varphi_{H2S(g)}$ the fugacity coefficient. The fugacity coefficient of H_2S in the gas mixture was calculated to be 0.33 with the Peng-Robinson equation of state which has been implemented into the Thermosolve software (Barnes, 2007; Koretsky, 2004; Peng & Robinson, 1976; Richard et al., 2005). The partial pressure of H_2S is 22 bar and results in a fugacity of 7.3 bar. This value lies in the range of fugacities calculated for carbonate reservoirs in the Alberta Basin (Richard et al., 2005). It has been suggested that these fugacities are controlled by metastable equilibrium between hydrocarbons, organic sulphur compounds and elemental sulfur (Richard et al., 2005). All these compounds are also present in the Madison Formation in the LaBarge Field and hence it is likely that a metastable equilibrium between the same compounds controls the H_2S fugacity.

The fluid composition in the reservoir has been reported for well Unit 22-19 (Blondes et al., 2016) (Figure 1). This fluid composition is similar to the fluid reported for the Whiskey Buttes Field further south along the Moxa Arch (Figure 1, Table 1) (Blondes et al., 2016). These fluids are characterized by a higher HCO_3^- and SO_4^{2-} concentrations but lower Ca^{2+} concentrations compared to fluids from wells penetrating the Madison Formation away from the Moxa Arch area in the Greater Green River Basin (Table 1) (Blondes et al., 2016). Initial fluid concentrations were set to those measured in well Unit 19-22 with the exception for HCO_3^-, SO_4^{2-} and Mg^{2+}. The HCO_3^- concentration is excessively high due to the equilibration with the CO_2 in the reservoir. Therefore we used the average concentration from wells outside the Moxa Arch (Table 2) (Blondes et al., 2016). The initial Mg^{2+} and SO_4^{2-} concentrations were set in equilibrium with dolomite and anhydrite, respectively (Table 2). The chlorine concentration acted as a charge balance throughout the reaction path.

Table 1

Field	Depth [m]	pH	HCO_3^- [mg/L]	Ca^{2+} [mg/L]	Cl^- [mg/L]	Fe^{2+} [mg/L]	K^+ [mg/L]	Mg^{2+} [mg/L]	Na^+ [mg/L]	SO_4^{2-} [mg/L]
Whiskey Butte	5224	7.9	8330	305	2758		94	36	6817	4938
LaBarge Unit 19-22	4229	7.9	5226	247	3894			100	8888	10174
Wildcat	4867		2635	848	43400		1852	391	27188	1800
Leroy	1777	7.2	2270	816	8181			337	6438	3863
Wertz	1798	7.0	1586	682	5112	1	198	118	4311	2921
Whitney Canyon	2975	7.5	1170	536	11200			132	8081	2600
Brady	4626	6.5	1006	3283	70737		4560	98	39961	750
Lost soldier	1792	7.6	937	1149	7604		243	386	4459	2764
Horse Trap	1686	8.8	556	335	663		47	1	3832	7417
Table Rock		4.4	378	6335	33400		1755	845	11939	85

Table 1 Average fluid composition of the Madison Formation water (Appendix 1) in different locations within the Greater Green River Basin (Figure 1a).

Table 2

Model	Stage	Temperature [C]	pH	HCO_3^- [mg/L]	Ca^{2+} [mg/L]	Cl^- [mg/L]	Na^+ [mg/L]	SO_4^{2-} [mg/L]	Fe^{2+} [mg/L]	Mg^{2+}	Methionine titrated [mol]	CO_2 titrated [mol]
Model 1 part 1	initial	175	5.6	1300	250	3894	8888	220	1	17	0.145	
Model 1 part 1	end	175	5.6	1002	54	9000	9540	1000	1.E-10	4.0		
Model 1 part 2	initial	200	5.6	9026 as CO_2(aq)	54	9000	9540	19880 as H_2S(aq)	1.E-10	3.0		0.5
Model 1 part 2	end	200	5.6	3810 as CO_2(aq)	18	8970	9370	19880 as H_2S(aq)	1.E-10	2		
Model 2	initial	200	5.6	1300	250	3894	8888	110	1	13	0.145	0.5
Model 2	end	200	5.6	29000 as CO_2(aq)	21	7000	9620	18250 as H_2S(aq)	2.00E-10	3		

Table 2 Fluid composition at the beginning and end of model 1 and 2.

We conducted the modelling with the react module and the V8R6 themodynamic database within Geochemist's Workbench® (GWB) software (Appendix 3). In model 1, the burial related TSR process was simulated as a titration model where methionine (aq) was titrated into the fluid at 175 °C, initially in equilibrium with dolomite and anhydrite, until 20 cm^3 of calcite precipitated (Table 2). The resulting fluid was then reacted with 0.5 mol of CO_2 (g) at 200 °C and 1 cm^3 of anhydrite (Table 2). The anhydrite was added at the onset of CO_2 addition to simulate the reaction of any remaining sulphate. For model 2, the TSR triggered by CO_2 model, the same amount of methionine (aq) and CO_2 (g) were titrated simultaneously into the fluid at 200 °C, initially in equilibrium with dolomite and anhydrite (Table 2). We chose 200 °C as a CO_2 influx temperature in order to not overestimate it and to be in agreement with primary fluid inclusion homogenisation temperature data (Zwahlen et al., 2019). In all cases the Eh was kept fixed during the reaction path since it controlled by the sulphur species and buffered by the H_2S(g) concentration (Kaszuba et al., 2011). We chose methionine as an organic compound because it includes sulphur which is in agreement with solid bitumen analysis (King et al., 2014). Parts of the organo-sulfur in the solid bitumen are likely from the original oil. However in terms of sulphur mass balance the sulphur in methionine plays a very minor role compared to the vast amount of anhydrite that gets consumed. Methionine also contains nitrogen, which results in an overestimation of gaseous nitrogen; however, the database doesn't list an organosulphur compound without nitrogen such as cystine. For the stable isotope fractionation modelling, we updated the GWB stable isotope database (Appendix 2). For the sulphate fractionation we used equilibrium and kinetic fractionation factors (Kiyosu & Krouse, 1990b; Ohmoto & Rye, 1979). We choose a $\delta^{34}S$ composition for anhydrite of 15‰, in agreement with Mississippian sulphate and carbonate-associated sulphate measured in pre-TSR calcite in the LaBarge Field (Zwahlen et al., 2019). The sulphur isotopic composition of methionine was set to the average phosphoria oil composition of 1‰ (King et al., 2014; Orr, 1974). The minerals were segregated from isotopic exchange with the fluid unless they dissolved or precipitated.

Modelling results

The oxygen fugacity of the models, constrained by the calculated H_2S fugacity, resulted in the Hm-Mt buffer (Figure 6). This is close to oxygen fugacities calculated for other carbonate reservoirs and is much larger than has been estimated for clastic reservoirs (Figure 6) (Helgeson et al., 1993; Richard et al., 2005). It remains unclear whether the difference in oxygen fugacities between carbonate and clastic reservoirs is an effect of thermodynamic dataset inconsistency (Richard et al., 2005).

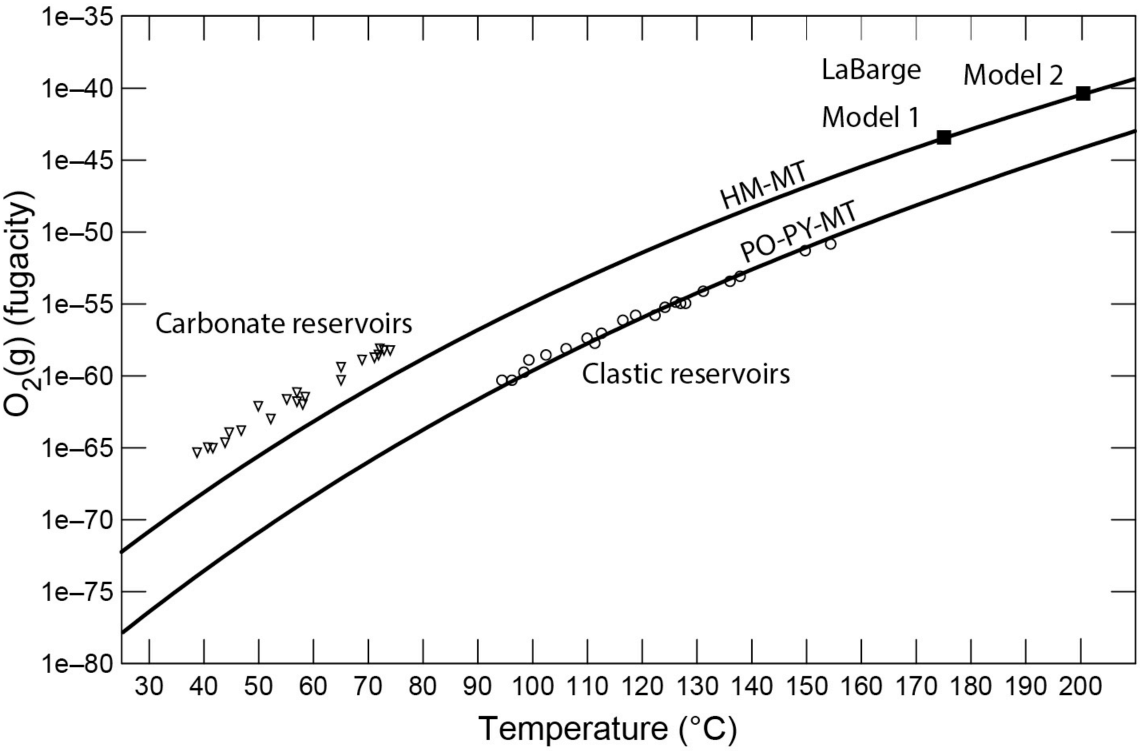

Figure 6 Oxygen fugacity calculated for the LaBarge reservoir (filled square) compared to other carbonate (triangles) (Richard et al., 2005) and clastic (circles) reservoirs (Helgeson et al., 1993). The curves correspond to the O_2(g) fugacities set by the hematite-magnetite (HM-MT) and the pyrrhotite-pyrite-magnetite (PO-PY-MT) buffers.

In both models (model 1 & 2) the fluid evolved to higher dissolved carbon dioxide and hydrogen sulphide and lower calcium concentrations (Table 2). The two models show distinctly different mineralogical results (Figure 7). In the burial- related TSR model (model 1) anhydrite dissolved while 20 cm^3 calcite and elemental sulphur precipitated as a result of methionine titration (Figure 7a). Pyrite and dolomite remained saturated throughout the model, although pyrite precipitation is limited by the low amount of iron in the fluid. In the second part of this model (model 1) calcite precipitated as a consequence of CO_2 influx (Figure 7b). We also tested the CO_2 influx without the 1

cm^3 of anhydrite. This resulted in an equally saturated volume of calcite, however, less calcite precipitated due to the limiting amount of Ca^{2+} in the fluid. The porosity remained almost unchanged and increased by only 0.1% throughout the model.

Figure 7 Mineralogical results of the two titration models: a) model 1 part 1 with methionine titration including runs at 165°C, 175°C and 185°C b) model 1 part 2 with CO_2 influx and c) model 2 with simultaneous methionine titration and CO_2 influx.

In the CO_2-triggered TSR model (model 2) anhydrite also dissolved, along with calcite precipitation. However, with the same amount of methionine, more than 1 cm^3 anhydrite remained undissolved at the end of the reaction path and less than 19 cm^3 of calcite precipitated (Figure 7c). A further difference to model 1 is that elemental sulphur did not become saturated (Figure 7c). Since elemental sulphur precipitated in model 1 but not in model 2 we explored the effect of temperature on the saturation of elemental sulphur and ran the methionine titration of model 1 at different temperatures (Figure 7a). The results showed that elemental sulphur saturated at 165 °C whereas at 185 °C calcite was the only precipitating mineral (Figure 7a).

Additionally we investigated the isotopic fractionation of sulphur during the reaction paths, with pre-defined $\delta^{34}S$ isotopic values for the different phases, and compared it to existing mineral and gas stable isotope data (King et al., 2014; Zwahlen et al., 2019) (Figure 8). There was no fractionation expected for aqueous sulphate incorporation into calcite, therefore we can compare the measured carbonate associated sulphate (CAS) isotopic composition to the modelled aqueous sulphate isotopic composition (Burdett et al., 1989). The modelled extent of the sulphate fractionation depends on whether equilibrium or kinetic fractionation factors are used (Figure 8a) (Kiyosu & Krouse, 1990a; Ohmoto & Rye, 1979). The modelled sulphate fractionation with the kinetic fractionation factor overlaps completely with the extent of fractionation observed in carbonate associated sulphates measured in anhydrite-replacive calcite (15.3 to 22.7‰) (Zwahlen et al., 2019) (Figure 8a). Therefore the kinetic fractionation factor is used for the following fractionation calculation. The fractionation between aqueous and gaseous hydrogen sulphide is negligible above 150 °C which enables us to compare the measured gaseous isotopic H_2S composition to the modelled aqueous isotopic H_2S composition (Czarnacki & Hałas, 2012; Eldridge et al., 2016). The modelled $\delta^{34}S$ value of the aqueous hydrogen sulphide increased during the reaction path to close to 10‰, which is the measured composition for the gaseous H_2S in the reservoir (King et al., 2014) (Figure 8b). Hence there modelled aqueous hydrogen sulphide isotopic composition is in agreement with the reservoirs value.

Figure 8 a) Kinetic and equilibrium fractionation of sulphate in model 1 in comparison with measurements from the reservoir carbonate associated sulphate (15.3 to 22.7‰, grey area) (Zwahlen et al., 2019) and b) Isotopic evolution of aqueous sulphide in model 1 by contrast with gaseous hydrogen sulphide data from the reservoir (dotted line) (King et al., 2014).

Discussion

In terms of mineralogy, the two models differ mainly in the saturation of elemental sulphur and the amount of calcite that is precipitated. Model 1 predicts the mineralogy observed in the cores, specifically calcite, elemental sulphur and pyrite. Elemental sulphur doesn't saturate when the model is run above 175 °C. This indicates that TSR likely occurred at ≤ 175 °C. The lower amount of dissolved anhydrite and precipitated calcite in model 2 could be related to the decreasing solubility of anhydrite with increasing temperature. Both models suggest that calcite precipitates as a consequence of CO_2 influx, not anhydrite as previously suggested (Kaszuba et al., 2011). All together model 1 represents the mineralogical data better than model 2. This indicates that the inititation of TSR was most likely related to temperature, and occurred at ≤ 175 °C. This is in agreement with the lowest primary fluid inclusion homogenisation temperatures measured in calcite that replaced anhydrite (Zwahlen et al., 2019). The modelled TSR process is more efficient at temperatures around 175°C compared to 200 °C due to the higher anhydrite solubility at lower temperatures. This might explain why TSR has not been observed at high temperature (≥ 200 °C) in the LaBarge Field and in other study areas (Biehl et al., 2016; Bildstein et al., 2001; Cai et al., 2001; Claypool & Mancini, 1989; Hao et al., 2015; Heydari & Moore, 1989; Jenden et al., 2015; Jiang et al., 2015; Liu et al., 2013;

Machel, 2001; Riciputi et al., 1994; Worden et al., 1995; Worden & Smalgeoley, 1996) and could indicate that there is an upper temperature limit for TSR.

Model 1 is further validated by consideration of the fractionation of the sulphur species present in the reservoir. The modelled fractionation of aqueous sulphate and hydrogen sulphide is consistent with mineral and gas data from the reservoir when a kinetic fractionation factor is used. The fractionation between the CAS sulphate isotopes has been previously related to fractionation during the reduction step (Meshoulam et al., 2016; Zwahlen et al., 2019). Therefore the modelled fractionation during the reduction step in agreement with the extent of fractionation of the CAS samples also confirms that reduction rather than diffusion is the rate limiting step (Meshoulam et al., 2016).

In both models the calcium concentration in the fluid limited the extent of calcite precipitation. The low calcium concentration in the modelled fluid is in agreement with the reported concentrations of the fluid from the LaBarge Field (Table 1). The high sulphate concentration in the reported fluid analysis suggests that calcium sulphate was not the limiting factor for TSR and that the calcium concentration is low due to calcite precipitation. The aqueous hydrogen sulphide concentration predicted by the models is extremely high but might be much lower in reality due to sorption onto organic matter or precipitation of more metal sulphides (King et al., 2014).

The insights regarding the initiation and mineralogical consequences of the TSR process based on reaction path modelling in the LaBarge Field could help to predict the occurrence of TSR elsewhere if fluid and mineral data are available. For geologic co-sequestration, these models show that anhydrite does not precipitate as a consequence of CO_2 addition into a reducing carbonate system. This disagrees with previous predictions (Kaszuba et al., 2011) and indicates that the H_2S concentration is solely diminished by sorption and sulphide precipitation. These results have to be taken into account when co-sequestration storage security is evaluated due to the reactive character of H_2S. However the insignificant porosity change is consistent with previous modelling results (Kaszuba et al., 2011), which is important for pressure predictions of co-sequestration scenarios.

Conclusion

Based on two simple reaction path models we explored the effect of burial related TSR and compared it to TSR triggered by hot CO_2 influx. Model 1, which assumed burial related TSR and subsequent CO_2 influx, correctly predicts the mineralogy observed in the core. On the other hand model 2 fails to saturate elemental sulphur. Therefore TSR at LaBarge was likely induced by burial and the CO_2 influx had no influence on TSR. Further both reaction path models suggest that the CO_2 influx leads to calcite precipitation instead of anhydrite as previously thought (Kaszuba et al., 2011).

This modelling approach is further validated by the agreement between sulphate and sulphide fractionation and the measurements of the corresponding phases in the reservoir. The output of the model adds additional constraints on the fluid history of the reservoir and can help predicting TSR elsewhere. In terms of geologic co-sequestration the modelled mineralogical consequences differ from previous predictions but are consistent with little porosity changes observed in previous models and have to be taken into account when assessing different co-sequestration scenarios.

However, more fluid analysis from wells in the LaBarge Field could improve the validity of the model. Additionally kinetic rate laws could be included into to the model to compare the rates of the different occurring processes such as dissolution and precipitation to the rate of sulphate reduction. Future research could also look at the complex fractionation processes of carbon and oxygen isotopes.

Acknowledgment

We thank the University of Manchester for funding this project.

Allis, R., Chidsey, T., Gwynn, W., Morgan, C., White, S., Adams, M., & Moore, J. (2001). Natural CO2 reservoirs on the Colorado Plateau and southern Rocky Mountains: Candidates for CO2 sequestration. *Proceedings of the First National Conference on Carbon Sequestration*, 14–17.

Barnes, C. S. (2007). *ThermoSolver: an integrated educational thermodynamics software program.*

Becker, T. P., & Lynds, R. (2012). A geologic deconstruction of one of the world's largest natural accumulations of CO2, Moxa arch, southwestern Wyoming. *AAPG Bulletin*, *96*(9), 1643–1664. https://doi.org/10.1306/01251211089

Bickle, M., Kampman, N., & Wigley, M. (2013). Natural analogues. *In DePaolo, D.J., et Al., Eds., Geochemistry of Geologic CO2 Sequestration: Reviews in Mineralogy and Geochemistry*, *77*(1), 15–71.

Biehl, B. C., Reuning, L., Schoenherr, J., Lüders, V., & Kukla, P. A. (2016). Impacts of hydrothermal dolomitization and thermochemical sulfate reduction on secondary porosity creation in deeply buried carbonates: A case study from the Lower Saxony Basin, northwest Germany. *AAPG Bulletin*, *100*(4), 597–621.

Bildstein, O., Worden, R. H., & Brosse, E. (2001). Assessment of anhydrite dissolution as the rate-limiting step during thermochemical sulfate reduction. *Chemical Geology*, *176*(1–4), 173–189. https://doi.org/http://dx.doi.org/10.1016/S0009-2541(00)00398-3

Blondes, M. S., Gans, K. D., Rowan, E. L., Thordsen, J. J., Reidy, M. E., Engle, M. A., et al. (2016). US Geological Survey National Produced Waters Geochemical Database v2. 2 (PROVISIONAL) Documentation. *US Geological Survey*.

De Bruin, R. H. (1991). Wyoming's carbon dioxide resources. *Open File Report*, *91–6*, 1–19.

De Bruin, R. H. (2001). Carbon dioxide in Wyoming, information pamphlet 8: Wyoming Geological Survey. *Laramie, Wyoming*, 1–11.

Budai, C., & Cummings, M. (1987). A depositional model of the Antelope Coal Field, Powder River

Basin, Wyoming. *Journal of Sedimentary Petrology*, *57*(1), 30–38. https://doi.org/10.1306/212F8A94-2B24-11D7-8648000102C1865D

Budai, J. (1985). Evidence for rapid fluid migration during deformation, Madison Group, Wyoming and Utah Overthrust Belt. *Rocky Mountain Carbonate Reservoirs — A Core Workshop [Golden, CO, August 10-11, 1985]*, 377–407. Retrieved from http://archives.datapages.com/data/sepm_sp/cw7/Evidence_of_Rapid_Fluid_Migration_during.pdf

Budai, J., Lohmann, K. C., & Owen, R. M. (1984). Burial dedolomite in the Mississippian Madison Limestone, Wyoming and Utah thrust belt. *Journal of Sedimentary Petrology*, *54*(1), 276–288. https://doi.org/10.1306/212F83FF-2B24-11D7-8648000102C1865D

Buoniconti, M. R. (2008). *The evolution of the carbonate shelf margins and fill of the Antler Foreland Basin by prograding Mississippian carbonates, Northern US Rockies*. *Open Access Dissertations*. Retrieved from http://scholarlyrepository.miami.edu/oa_dissertations/330

Burdett, J. W., Arthur, M. A., & Richardson, M. (1989). A Neogene seawater sulfur isotope age curve from calcareous pelagic microfossils. *Earth and Planetary Science Letters*, *94*(3), 189–198.

Cai, C., Hu, W., & Worden, R. H. (2001). Thermochemical sulphate reduction in Cambro–Ordovician carbonates in Central Tarim. *Marine and Petroleum Geology*, *18*(6), 729–741. https://doi.org/http://dx.doi.org/10.1016/S0264-8172(01)00028-9

Claypool, G. E., & Mancini, E. A. (1989). Geochemical relationships of petroleum in Mesozoic reservoirs to carbonate source rocks of Jurassic Smackover Formation, southwestern Alabama. *AAPG Bulletin*, *73*(7), 904–924.

Czarnacki, M., & Hałas, S. (2012). Ab initio calculations of sulfur isotope fractionation factor for H2S in aqua–gas system. *Chemical Geology*, *318–319*, 1–5.

https://doi.org/10.1016/j.chemgeo.2012.05.007

Eldridge, D. L., Guo, W., & Farquhar, J. (2016). Theoretical estimates of equilibrium sulfur isotope effects in aqueous sulfur systems: Highlighting the role of isomers in the sulfite and sulfoxylate systems. *Geochimica et Cosmochimica Acta*, *195*, 171–200. https://doi.org/10.1016/j.gca.2016.09.021

Hao, F., Zhang, X., Wang, C., Li, P., Guo, T., Zou, H., et al. (2015). The fate of CO2 derived from thermochemical sulfate reduction (TSR) and effect of TSR on carbonate porosity and permeability, Sichuan Basin, China. *Earth-Science Reviews*, *141*(0), 154–177. https://doi.org/http://dx.doi.org/10.1016/j.earscirev.2014.12.001

Helgeson, H. C., Knox, A. M., Owens, C. E., & Shock, E. L. (1993). Petroleum, oil field waters, and authigenic mineral assemblages Are they in metastable equilibrium in hydrocarbon reservoirs. *Geochimica et Cosmochimica Acta*, *57*(14), 3295–3339.

Heydari, E., & Moore, C. H. (1989). Burial diagenesis and thermochemical sulfate reduction, Smackover Formation, southeastern Mississippi salt basin. *Geology*, *17*(12), 1080–1084.

Huang, N. S., Aho, G. E., Baker, B. H., Matthews, T. R., & Pottorf, R. J. (2007). *Integrated reservoir modeling to maximize the value of a large sour-gas field with high concentrations of inerts: International Petroleum Technology Conference Paper 11202*. *IPTC conference in Dubai, UAE*.

Jenden, P. D., Titley, P. A., & Worden, R. H. (2015). Enrichment of nitrogen and 13C of methane in natural gases from the Khuff Formation, Saudi Arabia, caused by thermochemical sulfate reduction. *Organic Geochemistry*, *82*, 54–68. https://doi.org/10.1016/j.orggeochem.2015.02.008

Jiang, L., Cai, C., Worden, R. H., Li, K., Xiang, L., Chu, X., et al. (2015). Rare earth element and yttrium (REY) geochemistry in carbonate reservoirs during deep burial diagenesis: Implications for REY mobility during thermochemical sulfate reduction. *Chemical Geology*, *415*, 87–101.

Johnson, E. A. (2005). Geologic assessment of undiscovered oil and gas resources in the Phosphoria Total Petroleum System, southwestern Wyoming province, Wyoming, Colorado, and Utah. *US Geological Survey Southwestern Wyoming Province Assessment Team, Eds., Petroleum Systems and Geologic Assessment of Oil and Gas in the Southwestern Wyoming Province, Wyoming, Colorado, and Utah: US Geological Survey Digital Data Series DDS-69-D*.

Kampman, N., Bickle, M., Wigley, M., & Dubacq, B. (2014). Fluid flow and CO 2–fluid–mineral interactions during CO 2-storage in sedimentary basins. *Chemical Geology*, *369*, 22–50.

Kaszuba, J. P., Navarre-Sitchler, A., Thyne, G., Chopping, C., & Meuzelaar, T. (2011). Supercritical carbon dioxide and sulfur in the Madison Limestone: A natural analog in southwest Wyoming for geologic carbon–sulfur co-sequestration. *Earth and Planetary Science Letters*, *309*(1–2), 131–140. https://doi.org/http://dx.doi.org/10.1016/j.epsl.2011.06.033

Katz, D. A. (2008). Early and Late Diagenetic Processes of Mississippian Carbonates , Northern U . S . Rockies. *Open Access Dissertations*, *Paper 154*. Retrieved from http://scholarlyrepository.miami.edu/oa_dissertations/154/

Katz, D. A., Eberli, G. P., Swart, P. K., & Smith, L. B. (2006). Tectonic-hydrothermal brecciation associated with calcite precipitation and permeability destruction in Mississippian carbonate reservoirs, Montana and Wyoming. *AAPG Bulletin*, *90*(11), 1803–1841. https://doi.org/10.1306/03200605072

Katz, D. A., Buoniconti, M. R., Montañez, I. P., Swart, P. K., Eberli, G. P., & Smith, L. B. (2007). Timing and local perturbations to the carbon pool in the lower Mississippian Madison Limestone, Montana and Wyoming. *Palaeogeography, Palaeoclimatology, Palaeoecology*, *256*(3), 231–253.

King, H. E., Walters, C. C., Horn, W. C., Zimmer, M., Heines, M. M., Lamberti, W. A., et al. (2014). Sulfur isotope analysis of bitumen and pyrite associated with thermal sulfate reduction in reservoir carbonates at the Big Piney–La Barge production complex. *Geochimica et Cosmochimica Acta*, *134*, 210–220.

Kiyosu, Y., & Krouse, H. R. (1990a). The role of organic acid in the abiogenic reduction of sulfate and the sulfur isotope effect. *Geochemical Journal*, *24*(1), 21–27. https://doi.org/10.2343/geochemj.24.21

Kiyosu, Y., & Krouse, R. H. (1990b). The role of organic and acid the in the sulfur abiogenic isotope reduction effect. *Geochemical Journal*, *24*, 21–27. Retrieved from http://jlc.jst.go.jp/DN/JALC/00004729259?from=Google

Koretsky, M. D. (2004). *Engineering and chemical thermodynamics* (Vol. 2). Wiley Hoboken, NJ.

Liu, Q. Y., Worden, R. H., Jin, Z. J., Liu, W. H., Li, J., Gao, B., et al. (2013). TSR versus non-TSR processes and their impact on gas geochemistry and carbon stable isotopes in Carboniferous, Permian and Lower Triassic marine carbonate gas reservoirs in the Eastern Sichuan Basin, China. *Geochimica et Cosmochimica Acta*, *100*, 96–115.

Machel, H. G. (2001). Bacterial and thermochemical sulfate reduction in diagenetic settings—old and new insights. *Sedimentary Geology*, *140*(1), 143–175.

Meshoulam, A., Ellis, G. S., Said Ahmad, W., Deev, A., Sessions, A. L., Tang, Y., et al. (2016). Study of thermochemical sulfate reduction mechanism using compound specific sulfur isotope analysis. *Geochimica et Cosmochimica Acta*, *188*, 73–92. https://doi.org/http://dx.doi.org/10.1016/j.gca.2016.05.026

Obidi, O. (2014). *Timescales for the development of thermodynamic equilibrium in hydrocarbon reservoirs*. Imperial College London.

Ohmoto, H., & Rye, R. O. (1979). *Isotopes of sulfur and carbon. Geochemistry of Hydrothermal Ore Deposits (Barnes, HL, ed.)*. John Wiley & Sons Inc., New York.

Orr, W. L. (1974). Changes in sulfur content and isotopic ratios of sulfur during petroleum maturation--study of Big Horn basin Paleozoic oils. *AAPG Bulletin*, *58*(11), 2295–2318.

Peng, D.-Y., & Robinson, D. B. (1976). A new two-constant equation of state. *Industrial & Engineering Chemistry Fundamentals*, *15*(1), 59–64.

Richard, L., Neuville, N., Sterpenich, J., Perfetti, E., & Lacharpagne, J. C. (2005). Thermodynamic analysis of organic/inorganic reactions involving sulfur: Implications for the sequestration of H2S in carbonate reservoirs. *Oil & Gas Science and Technology*, *60*(2), 275–285.

Riciputi, L. E. E. R., Macheu, H. G., & Colp, D. R. (1994). An ion microprobe study of diagenetic carbonates in the devonian nisku formation of Alberta, Canada. *Geochimica et Cosmochimica Acta*, (1), 115–127. Retrieved from http://www.sciencedirect.com/science/article/pii/0016703796831334

Roberts, L. N. R., Lewan, M. D., & Finn, T. M. (2005). Burial history, thermal maturity, and oil and gas generation history of petroleum systems in the southwestern Wyoming province, Wyoming, Colorado and Utah. *US Geological Survey Southwest Wyoming Province Assessment Team: Petroleum Systems and Geologic Assessment of Oil and Gas in the Southwestern Wyoming Province, Wyoming, Colorado, and Utah: US Geological Survey Digital Data Series DDS-69-D*.

Smith, L. B., Eberli, G. P., & Sonnenfeld, M. (2004). Sequence-stratigraphic and paleogeographic distribution of reservoir-quality dolomite, Madison Formation, Wyoming and Montana. *Integration of Outcrop and Modern Analogs in Reservoir Modeling, AAPG Memoir 80*, *80*, 67–92. https://doi.org/10.1306/61EED030-173E-11D7-8645000102C1865D

Sonnenfeld, M. (1996). *An Integrated Sequence Stratigraphic Approach to Reservoir Characterization* *of the Lower Mississippian Madison Limestone, Emphasizing Elk Basin Field, Bighorn Basin, Wyoming and Montana*. Colorado School of Mines. Retrieved from https://books.google.co.uk/books?id=g4TatwAACAAJ

Stilwell, D. P. (1989). CO2 resources of the Moxa Arch and the Madison Reservoir, 105–115.

Williams, R. H., & Paulo, S. (2002). Major Roles for Fossil Fuels in an Environmentally Constrained World. *Sustainability in Energy Production and Utilization in Brazil: The next Twenty Years*, *2002*(February), 18–20. Retrieved from http://www.feagri.unicamp.br/energia/energia2002/jdownloads/pdf/papers/paper_Williams.pdf

Worden, R. H., & Smalgeoley, P. C. (1996). H 2 S-producing reactions in deep carbonate gas reservoirs: Khuff Formation, Abu Dhabi. *Chemical Geology*, *133*(1), 157–171.

Worden, R. H., Smalley, P. C., & Oxtoby, N. H. (1995). Gas souring by thermochemical sulfate reduction at 140 C. *AAPG Bulletin*, *79*(6), 854–863.

Zwahlen, C., Hollis, C., Lawson, M., Becker, S. P., Boyce, A., Zhou, Z., & Holland, G. (2019). Constraining the Fluid History of a CO2-H2S Reservoir: Insights From Stable Isotopes, REE, and Fluid Inclusion Microthermometry. *Geochemistry, Geophysics, Geosystems*, *20*(0). https://doi.org/10.1029/2018GC007900